

A *FUSE* Survey of Interstellar O VI Absorption in the Small Magellanic CloudCharles G. Hoopes¹, Kenneth R. Sembach^{1,2}, J. Christopher Howk¹, Blair D. Savage³,
and Alex W. Fullerton^{1,4}**ABSTRACT**

We present the results of a *Far Ultraviolet Spectroscopic Explorer (FUSE)* survey of O VI 1031.93 Å and 1037.62 Å absorption toward 18 OB stars in the Small Magellanic Cloud (SMC). The *FUSE* data are of very high quality, allowing a detailed study of the coronal temperature gas in the SMC. We find that O VI is ubiquitous in the SMC, with a detection along every sight line. The average value of the O VI column density in the SMC is $\log \langle N(\text{O VI}) \rangle = 14.53$. This value is 1.7 times higher than the average value for the Milky Way halo (perpendicular to the Galactic plane) of $\log N_{\perp}(\text{O VI}) = 14.29$ found by *FUSE*, even though the SMC has much lower metallicity than the Galaxy. The column density in the SMC is higher along sight lines that lie close to star-forming regions, in particular NGC 346 in the northern part of the SMC, and to a lesser degree the southwestern complex of H II regions. This correlation with star formation suggests that local processes have an important effect on the distribution of coronal gas in the SMC. If the sight lines within NGC 346 are excluded, the mean column density for the SMC is $\log N(\text{O VI}) = 14.45$, only 1.4 times higher than the Milky Way average. The standard deviation of the column densities for sight lines outside of NGC 346 is $\pm 27\%$, somewhat lower than the deviation seen in the Milky Way halo. The lowest O VI column densities, $\log N(\text{O VI}) \sim 14.3$, occur in the central region and in the southeastern “Wing” of the galaxy. Even these low column densities are as high as the Milky Way average, establishing the presence of a substantial, extended component of coronal gas in the SMC. The O VI absorption is always shifted to higher velocities than the main component of lower ionization gas traced by Fe II absorption. The O VI line widths are broader than expected for pure thermal broadening at 3×10^5 K, the temperature at which the O VI peaks in abundance, so large non-thermal motions or multiple hot gas components are likely present. We discuss several mechanisms that may be able to explain the observed properties of the hot gas, including supershells, a galactic fountain, and the infall of gas previously stripped from the SMC by tidal interactions with the Milky Way and the Large Magellanic Cloud. If a galactic fountain produces the hot gas, the mass flux per unit surface area is $\dot{M}/\Omega \sim 2 \times 10^{-2} \text{ M}_{\odot} \text{ yr}^{-1} \text{ kpc}^{-2}$.

Subject headings: ISM: atoms — galaxies: Magellanic Clouds — galaxies: ISM — ultraviolet: ISM

¹Department of Physics and Astronomy, Johns Hopkins University, 3400 N. Charles St., Baltimore, MD 21218; choopes@pha.jhu.edu, howk@pha.jhu.edu, awf@pha.jhu.edu

²Current address: Space Telescope Science Institute, 3700 San Martin Dr., Baltimore, MD 21218; sembach@stsci.edu

³Department of Astronomy, University of Wisconsin-Madison, 475 North Charter Street, Madison, WI 53706; savage@astro.wisc.edu

⁴Department of Physics and Astronomy, University of Victoria, P.O. Box 3055, Victoria, BC V8W 3P6, Canada

1. Introduction

The O VI 1031.93 Å and 1037.62 Å lines are important diagnostics of the processes responsible for distributing mass and energy in the interstellar medium (ISM). O VI is difficult to produce through photoionization, requiring photons with $h\nu \geq 114$ eV. Gas containing O VI is therefore most likely collisionally ionized. Since O VI peaks in abundance at 3×10^5 K (Sutherland & Dopita 1993), an unstable region of the cooling curve, gas containing O VI is either cooling from higher temperatures, or being heated. As such, it is a useful probe of energetic processes in the ISM including shock heating (Shull & McKee 1979), conductive heating and cooling (Borkowski, Balbus, & Fristrom 1990), and turbulent mixing layers (Slavin, Shull, & Begelman 1993). Coronal gas traced by O VI is intermediate in temperature between the very hot ($T \sim 10^{6-7}$ K) X-ray emitting gas and the warm ($T \sim 10^4$ K) ionized medium.

Opportunities to observe the O VI lines have been limited. The first observations of O VI were made with the *Copernicus* satellite along sight lines toward nearby bright stars ($V \leq 7$, $d \lesssim 2000$ pc) (Jenkins & Meloy 1974; Jenkins 1978a,b). Later observations were possible with the ORFEUS-SPAS missions (Hurwitz & Bowyer 1996; Hurwitz et al. 1998; Widmann et al. 1998; Sembach, Savage, & Hurwitz 1999). These observations, combined with observations of C IV $\lambda\lambda 1548.20, 1550.77$, N V $\lambda\lambda 1238.82, 1242.80$, and Si IV $\lambda\lambda 1393.76, 1402.77$, have built upon the original idea of a Galactic corona of hot gas which provides pressure confinement for high-latitude clouds (Spitzer 1956). While results for C IV, N V, and Si IV have greatly increased our understanding of the Galactic corona, the relative lack of information on O VI has been frustrating, since it probes a hotter temperature range and is less likely to be produced by photoionization.

With the launch of the *Far Ultraviolet Spectroscopic Explorer (FUSE)* in 1999 (Moos et al. 2000), access to the O VI lines has returned. *FUSE* is much more sensitive than *Copernicus*, allowing more distant stars and extragalactic sources to be observed. One of the major science goals of *FUSE* is to study the properties and distribution of hot gas in the local universe through O VI absorption. Early results have already been published for the Galactic halo and high velocity clouds (Savage et al. 2000; Sembach et al. 2000), and more comprehensive surveys are in progress.

The sensitivity of *FUSE* makes it possible to observe early type stars in the Magellanic Clouds, so we can now study the O VI absorption in galaxies with different properties than our own. The Small Magellanic Cloud (SMC) has properties that are vastly different from the Milky Way. It has low mass, low metallicity, and it is currently undergoing a gravitational interaction with two more massive galaxies. These factors may influence the properties of hot gas in the ISM of the SMC. The hot gas in the SMC has been studied previously using *International Ultraviolet Explorer (IUE)* spectra (de Boer & Savage 1980; Fitzpatrick & Savage 1983; Fitzpatrick 1984, 1985; Fitzpatrick & Savage 1985). Absorption by C IV and Si IV was measured toward the nine stars studied by Fitzpatrick & Savage (1985), who found evidence for a global component of highly ionized gas. More recently, Space Telescope Imaging Spectrograph (STIS) spectra of one of the sight lines studied by Fitzpatrick & Savage (1985), AV229 (HD 5980), were analyzed by Koenigsberger et al. (2001) and Hoopes et al. (2001), who also found evidence for hot gas in a supernova remnant in addition to the general ISM. The spectra show absorption by N V in addition to C IV and Si IV. *FUSE* data on O VI toward Sk 108 in the SMC has already been analyzed by Mallouris et al. (2001), but the complicated stellar continuum prevented an accurate determination of the O VI column density. Wang (1991) and Wang & Wu (1992) discovered an X-ray halo around the SMC using *Einstein* data, with spectral properties that suggest the presence of hot, thermal ISM components.

In this paper we present the results of a *FUSE* O VI absorption survey of 18 stars in the SMC. By observing stars in a variety of environments in the SMC, we search for a global component of hot gas, as

well as clues to the origins of the highly ionized gas. In section 2 we describe the observations and data processing. Section 3 describes the O VI content of the SMC, its variation with location, and a comparison to the Milky Way. The kinematics of the O VI absorbing gas are described in section 4, and section 5 contains a discussion of the observed O VI absorption. Section 6 summarizes the primary conclusions of our study. In a parallel effort, Howk et al. (2002) present a study of O VI absorption in the Large Magellanic Cloud.

2. Observations and Data Reduction

We obtained *FUSE* spectra of early type stars in 18 locations in the SMC. Table 1 lists the names and properties of the stars used in this project. For information on the local interstellar environment of these stars, see Danforth et al. (2002). The star names are from Azzopardi & Vigneau (1982) and Sanduleak (1968, 1969). The NGC 346 identifiers are from Walborn & Blades (1986), Walborn et al. (1995), and Massey, Parker, & Garmany (1989), and the new spectral type for NGC346–3 is from Walborn et al. (2001a). The parameters of the *FUSE* observations are given in Table 2. All of the spectra were taken through the large (LWRS) apertures, which are $30'' \times 30''$ in size. The *FUSE* instrument consists of four channels, two optimized for short ultraviolet wavelengths (SiC1 and SiC2: 905–1100 Å) and two optimized for longer ultraviolet wavelengths (LiF1 and LiF2: 1000–1187 Å). The O VI lines are covered by all four channels, but the LiF1 channel is the most sensitive; it is the primary channel considered here, although all of the results were verified with the LiF2 data. Because of fixed pattern features in the detectors, we required that any absorption line be present in these two channels to be considered a real feature. The LiF1 spectra in the wavelength region containing the O VI lines are shown in Figure 1.

The raw time-tagged photon event lists for each individual exposure were combined and run through the standard *FUSE* calibration pipeline (CALFUSE v1.8.7) available at Johns Hopkins University. The pipeline screens data for passage through the South Atlantic Anomaly and low Earth limb angle pointings and corrects for thermal drift of the gratings, thermally induced changes in the detector read-out circuitry, and Doppler shifts due to the orbital motion of the satellite. Finally the pipeline subtracts a constant detector background and applies wavelength and flux calibration. The velocity zero-point was set by shifting the spectrum so that the Milky Way component of the H₂ and low ionization lines lie at a Local Standard of Rest (LSR) velocity of 0 km s^{−1}, based on the results of Mallouris et al. (2001). The spectra were binned by three pixels (~ 6 km s^{−1} near O VI), and the nominal resolution of the data is ~ 20 km s^{−1} (FWHM). The wavelength solution is accurate to ~ 6 km s^{−1} on average, although deviations of 10–15 km s^{−1} may exist over small regions of the spectrum.

The four sight lines in NGC 346 present an additional complication. The four stars *FUSE* observed are separated by only a few arcseconds, so the light of all four stars, and perhaps others, entered the LWRS apertures and is present in the spectrum of each star. The resultant spectra are blends of several stars, with broadened absorption features due to the positional offsets of the sources in the apertures. The four spectra in this region look very similar, with minor differences probably caused by shifting a small number of fainter stars in or out of the aperture at the different pointings. Although we analyzed each sight line separately, the reader should recognize that the results for these four sight lines are correlated. When determining global properties of the SMC or Milky Way, we averaged the results for these four sight lines, and treated them as one measurement. In a future paper we will report on new *FUSE* observations of the NGC 346 stars using smaller apertures to isolate the individual stars.

3. Column Densities

3.1. Measurements

Equivalent widths and column densities were measured using the procedures described by Sembach & Savage (1992). The total column densities were derived by summing the apparent optical depth over the velocity range of the O VI 1031.93 Å line. The O VI 1037.62 Å line was blended with other lines in all of the spectra, rendering it useless for determining O VI column densities. The apparent optical depth method is valid as long as there is no unresolved saturated structure in the line. The high temperatures required for O VI would result in a thermal line width of $\approx 30 \text{ km s}^{-1}$ (FWHM), larger than the *FUSE* line spread function width ($\approx 20 \text{ km s}^{-1}$), so the O VI lines should be resolved. No saturated O VI lines were seen in the *FUSE* data, so we conclude that the absorption is optically thin.

Uncertainties in the equivalent widths and column densities were evaluated very conservatively. For each spectrum we first placed a nominal continuum over the O VI 1031.93 Å line by fitting low order (≤ 5) Legendre polynomials to the nearby stellar continuum. Continuum error estimates were calculated according to the prescription outlined by Sembach & Savage (1992). However, due to the high degree of continuum curvature and systematic uncertainties caused by possible stellar absorption near some of the profiles, we explored a wider range of parameter space in the continuum fits than was suggested by the formal (objective) approach. To do this we varied the continuum fit to the most extreme values above and below the nominal fit that were still reasonable continuations of the nearby continuum. These bracketing continuum placements are shown in Figure 1 as dashed lines, while the nominal fits are shown as solid lines. While this method adds a more subjective element to the evaluation of uncertainties, the potentially drastic effect of errors in the continuum placement justify such a conservative approach.

We used the 6-0 P(3) 1031.20 Å and 6-0 R(4) 1032.35 Å lines of H₂, which are close to the O VI line, to test whether the continuum fits were reasonable. To do this we fit a Gaussian function to nearby H₂ lines from the same rotational level having similar values of $f\lambda$, and plotted the fits at the positions of the H₂ lines near O VI. The fits are plotted in Figure 2, which show the continuum-normalized O VI lines using the nominal continuum fits. In most cases the fits matched the observed lines using the nominal continuum fit. In some of the spectra there is a stellar feature that falls on the 6-0 P(3) 1031.195 Å line (*e.g.*, AV378). This feature appears to be correlated in strength with another feature at $\sim 1033.5 \text{ Å}$. Other cases where the H₂ line fit did not match the data are discussed below. All O VI measurements were carried out using the three continuum fits in order to evaluate the uncertainties resulting from errors in the continuum placement. The presence of variable features in the stellar winds of the stars can cause substantial errors in the derived O VI column densities by affecting the continuum placement (Lehner et al. 2001). We have not made any attempt to correct for this directly, but the sample was defined by choosing stars that appeared to have relatively simple continua around the 1032 Å line.

The H₂ model for AV69 did not match the 6-0 R(4) 1032.351 Å line. This star has a peculiar metallicity, which can affect the shape of the stellar wind lines (Walborn et al. 2000). To test the hypothesis that the peculiar wind lines have compromised our continuum fit, we have examined the STIS spectrum of AV69, along with eight other stars in the *FUSE* sample that have been observed by STIS (Walborn et al. 2000). While the C IV lines show a normal P-Cygni wind profile, the N V lines have very weak and relatively narrow wind profiles (Walborn et al. 2000). If the O VI stellar wind profile is shaped similarly, it would hinder the measurement of the interstellar O VI. This would explain the lack of agreement between the H₂ model and the observed spectrum. These tests lead us to distrust the interstellar O VI column density measured toward AV69, which would be the largest in the SMC if the continuum fit were correct. The H₂ models for AV14 and

AV26 also did not match the observed spectra well. Unfortunately these two stars have not been observed by STIS, so we cannot be sure if there is contamination by stellar absorption. Absorption by O VI in the SMC at high velocities could also produce this effect. Nevertheless, these sight lines are suspicious, and while the measurements are included with those of the other sight lines, the reader is warned to interpret the results for these three stars with caution. For global properties we computed averages both with and without AV14 and AV26. AV69 is not included in the global averages as it is clearly not reliable.

A nominal velocity integration range was chosen for the Milky Way and SMC components of O VI in each spectrum. We chose the velocity of the point of lowest apparent optical depth between the two components to be the boundary for the integration limits. If the two components are described by overlapping Gaussian functions, the approach could shift some of the column density from the stronger component to the weaker component. Tests using Gaussian fits to several of the sight lines revealed that this effect is $\lesssim 3\%$ in the worst cases, and $\lesssim 1\%$ in typical cases. To account for this effect, as well as possible H₂ absorption on either side of the O VI 1032.93 Å line, we varied the velocity integration limits by $\pm 5 \text{ km s}^{-1}$ so that the total integration range was 10 km s^{-1} larger or smaller than the nominal limits. The variation in column density found with this method was greater than the effect of the overlapping Gaussian profiles. This uncertainty was combined with the fixed-pattern noise uncertainty in the *FUSE* spectra. The measured equivalent widths and column densities for the Milky Way and the SMC components are listed in Tables 3 and 4. The first quoted uncertainty is that due to fixed pattern noise and velocity range errors, and the second shows the effects of varying the continuum placement (as indicated in Figure 1), which in the majority of cases is the dominant source of uncertainty.

3.2. Results

It is immediately clear from the spectra shown in Figures 1 and 2 that the O VI absorption from the SMC is usually much stronger than that in the Milky Way along the same line of sight. O VI is detected in both the Milky Way and the SMC along every SMC sight line observed by *FUSE*, including the sight line toward Sk 188, which is in the periphery of the SMC. This suggests that a widespread component of coronal temperature gas is present in the SMC. The measured equivalent widths, column densities, line widths, and positions are given in Tables 3 and 4 for the Galactic and SMC absorption, respectively.

Figure 3 shows the locations of the *FUSE* targets on an H α image of the SMC (Gaustad et al. 2001). The stars are marked with circles denoting the O VI column density, and are labeled by the identification number from Table 1. The largest star-forming region in the SMC is NGC 346, in the northern part of the galaxy at the location of star 8 in Figure 3. Four of the targets are in this H II region, and several others lie close to it. There is another concentration of H II regions in the southwest corner of the SMC, also sampled by several *FUSE* sight lines. The central and the southeastern parts of the galaxy are much less actively forming stars. The southeastern extension is sometimes called the “Wing”, while the northern and southwestern parts make up the “Bar.” Most of the star formation in the SMC is occurring in the Bar (Kennicutt et al. 1995).

The largest O VI column densities occur near the star-forming regions. Figure 4 shows the distribution of $\log N(\text{O VI})$ with distance from NGC 346. The column toward AV229 (Sk 78, HD5980) is the highest (excluding AV69, which may be compromised by stellar absorption), with $\log N(\text{O VI})=14.86$. The sight line to AV229 passes through a supernova remnant (SNR) in the SMC (Koenigsberger et al. 2001), which contributes roughly one third of the total O VI column (Hoopes et al. 2001). Even if the contribution of

the SNR is excluded, the O VI column is one of the highest in the SMC, with $\log N(\text{O VI})=14.68$. AV229 is on the edge of NGC 346, and high columns are seen toward stars in and around this H II region (AV232 and the NGC 346 stars). The stars outside of NGC 346 in the northern end of the Bar are markedly lower, however. The O VI column toward AV321 (star 12) is still relatively high, but the value for AV378 (star 13) is low compared to most of the other stars in the sample.

The highest points outside of NGC 346 are the points in the star-forming regions in the southwestern end of the Bar, marked by open circles in Figure 4. The three highest values in this direction are found for AV69, AV14, and AV26, all of which may be contaminated by stellar absorption and are not shown in Figure 4. If these are left out, three of the remaining sight lines in this area (AV95, AV75, and AV15, stars 7, 5, and 2) still show large O VI columns, but not as large as those near NGC 346, and one star (AV83, star 6) is fairly low. The H II regions in this part of the SMC are not forming stars as actively NGC 346, based on their H α luminosity (Kennicutt & Hodge 1986).

The columns toward stars in the central and southeastern parts of the SMC (AV235, AV423, and Sk 188, stars 11, 14, and 15) are lower than those in the other parts of the galaxy. These regions have much less star formation occurring (Kennicutt et al. 1995). While the columns are lower, they are still as high as the Milky Way component along the same sight lines. This is evidence for an extended component of O VI in the SMC, which is locally enhanced by processes related to star formation, such as SNRs. The O VI column density of hot gas in the SMC rivals that of the Milky Way halo even in the absence of local enhancement, which is perhaps surprising in a small galaxy with low metallicity.

In Figure 4 the stars in and around NGC 346 stand out from the rest of the points. If these points are excluded, the mean column density in the SMC is $\log N(\text{O VI})=14.45\pm_{0.14}^{0.10}$. This is about 1.4 times higher than the mean value of the column density perpendicular to the Milky Way plane of $\log N_{\perp}(\text{O VI})=14.29$ (Savage et al. 2000). Not including the contribution from the SNR toward AV229, the column densities toward the NGC 346 stars, AV229, and AV232 are all very similar, almost identical within the uncertainties of the measurements (counting the NGC 346 stars as a single measurement). In the rest of the SMC there is more variation in the O VI column, in one case a factor of 2 difference between stars only a few arcminutes apart (AV83 and AV95, stars 6 and 7), which is about the same as the distance between the stars near NGC 346. The standard deviation in the column densities is about 27% (excluding the NGC 346 stars, AV229, and AV232), which is somewhat lower than the deviation seen in the Milky Way (Savage et al. 2000). In general, the O VI column density appears to vary on both large and small scales, with the exception being the smooth distribution near NGC 346.

4. Kinematics

We calculated the first and second moments of the O VI 1031.93 Å absorption line profiles in the Milky Way and the SMC. The first moment gives the average velocity of the line (weighted by the data values) and the second moment gives the line width, equivalent to the standard deviation (σ) if the line is Gaussian in shape. The line widths given in Tables 2 and 3 were converted to FWHM values by multiplying by 2.35. An initial concern was that measurement of these quantities would be hindered by the blending of the SMC and Milky Way components. In most cases the blue edge of the SMC absorption and the red edge of the Milky Way absorption were chosen as the midpoint of the shoulder between the two absorption peaks. Since part of the low-velocity end of the line profile is missing due to blending, the measured positions of the SMC lines may be weighted toward higher velocities. However, comparison of the position measured in this manner

with the visually determined absorption minimum revealed that such an effect did not occur, or was too small to be seen.

The O VI lines in the SMC are broader than the Milky Way O VI lines. The FWHM ranges from $82 - 115 \text{ km s}^{-1}$ with a mean of $94 \pm 9 \text{ km s}^{-1}$, compared to the mean $59 \pm 11 \text{ km s}^{-1}$ for the Milky Way line widths (which range from 40 to 66 km s^{-1}). Neither the NGC 346 stars nor AV69 were included in the mean values. The SMC mean line width corresponds to a temperature $T = 3.1 \times 10^6 \text{ K}$ if the width is due to thermal broadening alone, while the Milky Way mean line width corresponds to $T = 1.6 \times 10^6 \text{ K}$. In collisional ionization equilibrium, O VI peaks in abundance at $T = 3 \times 10^5 \text{ K}$ (Sutherland & Dopita 1993). If most of the gas is at this temperature, then either large non-thermal motions are required to contribute to the line broadening, or there are multiple components of O VI absorption in both galaxies.

Figure 5 compares the O VI line profiles to those of Fe II $\lambda 1144.94$. In many of the sight lines there are two low ionization absorption complexes in the SMC, a feature also seen in *IUE* spectra (Fitzpatrick 1985) and H I 21cm studies (McGee & Newton 1981; Mathewson, Ford, & Visvanathan 1988). Most of the absorption from the low ionization gas occurs in the lower velocity ($\sim +130 \text{ km s}^{-1}$) component (Danforth et al. 2002). The higher velocity ($\sim +180 \text{ km s}^{-1}$) component is most prominent in the southwest part of the Bar, and is not visible in the spectra of stars near NGC 346. The spectrum of AV423 does not show the double peaked profile, but the Fe II absorption is as wide as that in the AV235 spectrum, where the double peaked profile is strong. Thus, it is possible that both components are present but saturated toward AV423. This is not the case toward Sk 188, although the Fe II line is asymmetric toward the red side. Sk 188 is on the far eastern part of the SMC, quite isolated from the other stars in the sample.

The O VI absorption appears to lie close to the velocity of the $+180 \text{ km s}^{-1}$ component of low-ionization absorption in those sight lines where this component is visible, although there are a few cases where the O VI absorption peaks between the two components (AV26, AV14, AV15), and there are cases near NGC 346 where the peak is redward of both components (AV321, AV378). In several cases (AV378, AV321, AV83, and AV95) there may be structure in the O VI absorption corresponding to the two low ionization components, although the bulk of the absorption is still redward of the main low ionization component at $+130 \text{ km s}^{-1}$. In the sight lines where the $+180 \text{ km s}^{-1}$ low ionization component is not visible, the O VI is still systematically shifted to higher velocities than the main component of low ionization absorption. This indicates that the O VI absorbing gas has physically distinct properties from the gas producing most of the low ionization absorption.

5. Discussion

The observations described in this paper form a picture in which the SMC has a substantial, widespread component of hot gas. On average the O VI column density in the SMC is ~ 1.7 times that of the average column density perpendicular to the plane of the Milky Way of $\log N_{\perp}(\text{O VI}) \approx 14.29$ (Savage et al. 2000). The distribution of hot gas in the SMC appears to be strongly influenced locally by nearby star formation. The largest O VI column densities are measured along sight lines in or near star-forming regions. The distribution of hot gas is strongly affected by star formation in NGC 346, in particular, where the column density is ~ 1.7 times higher than the average for the rest of the SMC. The O VI column density in the SMC *excluding* NGC 346 is ~ 1.4 times larger than the Galactic average.

Comparisons between the SMC and the Milky Way can be misleading because the two galaxies have vastly different structures. It is not clear that the SMC can be described as a planar system, in which an

inclination correction would be necessary. The system of carbon stars in the SMC has been modeled as a plane with an inclination of 73° (Kunkel, Demers, & Irwin 2000). If this inclination holds for the hot gas component of the SMC, then $\log N_\perp(\text{O VI}) = 14.00$, and if NGC 346 is excluded $\log N_\perp(\text{O VI}) = 13.92$. The SMC exhibits evidence for a large depth, with estimates ranging from 3.3 to 14 kpc (see *e.g.*, Welch et al. 1987; Groenewegen 2000), with some estimates as high as 32 kpc (Mathewson, Ford, & Visvanathan 1986). The depth, optical appearance, and the double-peaked H I velocity profiles suggest that a simple planar model is not applicable. If the structure of the SMC is truly irregular, it is probably more appropriate to use the total column density, with no correction for inclination, for comparison with the Milky Way.

Multiple supernovae and stellar winds associated with H II regions are a likely mechanism to produce the enhanced O VI seen near star-forming regions in the SMC. Supernovae are thought to produce much of the hot gas in galaxies (McKee & Ostriker 1977; Spitzer 1990), and one supernova remnant observed by *FUSE* contains a large amount of O VI (Hoopes et al. 2001). In the Milky Way, O VI is higher than the Galactic average on the sight line to 3C 273, which probes the supernova remnant Loop IV (Sembach et al. 2001), although it is not enhanced above the Scutum supershell (Sterling et al. 2002). Several giant H II regions contain X-ray emitting gas, so they probably contain coronal phase gas as well (Williams & Chu 1995; Wang 1999). It is important to note that the average column density for the SMC may appear high compared to the Milky Way because several of the SMC sight lines pass through star-forming regions, while the Milky Way sight lines to extragalactic sources typically do not.

One might expect the low metallicity of the SMC to result in a lower O VI abundance. However, Edgar & Chevalier (1986) found that the metallicity has little effect on the column density of hot, radiatively cooling gas because the lower abundance is compensated by a longer cooling time. If the O VI in the SMC arises in radiatively cooling hot gas, our results confirm that low oxygen abundance does not reduce the O VI abundance. In fact, it is conceivable that the lower cooling efficiency could result in more hot gas, and thus a higher observed O VI column density. This was suggested by Wang (1991) to explain the soft X-ray halo.

The $+130 \text{ km s}^{-1}$ component of low-ionization gas is most often interpreted as being in front of the $+180 \text{ km s}^{-1}$ component (see Danforth et al. 2002). Extending this interpretation to the O VI absorbing gas would mean that it is behind most of the cooler gas. This interpretation is unsatisfactory for several reasons. The O VI is seen at higher velocities than the bulk of the low ionization material in nearly every sight line, requiring that every star in the sample be associated with the weaker of the low ionization components. In NGC 346, where the $+180 \text{ km s}^{-1}$ low ionization component is not visible, the O VI is still redshifted compared to the low ionization gas. There is no correlation between the strength of the $+180 \text{ km s}^{-1}$ component and the O VI column density; for example, the high velocity component is much more pronounced in the AV83 spectrum than in AV15, yet the O VI column toward AV15 is ~ 1.6 times higher than toward AV83. A correlation might be expected if the low ionization and high ionization gas are cospatial. In many of the spectra the O VI does not fall at the same velocity as the $+180 \text{ km s}^{-1}$ component. Although these facts do not preclude a physical association between the O VI and the $+180 \text{ km s}^{-1}$ low-ionization component, it is also possible that the similarity of their velocity distributions is coincidental.

Staveley-Smith et al. (1997) suggest that the appearance of two H I components in the SMC is due to the presence of shells and supershells along the line of sight, not due to distinct cloud complexes making up the SMC. In this scenario the hot gas seen in O VI absorption could lie between the two apparent components in velocity space if it fills the interior of the shells. If these shells are most numerous along the Bar where the star formation is concentrated, it would naturally explain the higher O VI column densities measured there. To test this idea we examined the sight lines that fall within shells listed in the catalog of Staveley-Smith et al. (1997). These sight lines are: AV75, AV83, and AV95 in the southwest (stars 8, 9, and 10), and AV321

and AV378 in the north (stars 12 and 13). There are also shells in the direction of AV14, AV26, and AV69, but we do not discuss these due to their uncertain O VI profiles. All of these sight lines are in the Bar, but there are other sight lines in the Bar and elsewhere in the SMC that do not pass through any catalogued shell. Staveley-Smith et al. (1997) point out that shells may have been missed in regions with complex H I distribution. For the sight lines in the direction of a shell, the shell velocities usually correspond to the peak of the O VI absorption, although not in every case (see Figure 5). However, on all five sight lines there is significant O VI absorption outside of the velocity range of the expanding shells. Furthermore, many of the sight lines are not in the direction of any shell. We conclude that hot gas in expanding shells produces some of the O VI absorption, but the bulk is produced in gas outside of the shells.

A galactic fountain might also explain the observations. In this scenario correlated supernovae produce a flow of very hot gas into the halo, which then cools and falls back on the main body of the galaxy. Absorption from O VI is produced as the gas cools through temperatures of $(1 - 3) \times 10^5$ K. If at this point the gas is falling back toward the SMC, a shift toward higher velocities from the low-ionization gas would be expected, as is seen in the data. This scenario might also explain the correlation with star formation, if the expelled gas remains close to the site of star formation. This might not be expected in a rotating disk system like the Milky Way, but would be more likely in the SMC, which appears to lack a coherent direction of rotation. Wang (1991) found diffuse X-ray emission in the SMC with spectral properties that favor an origin in hot gas, leading them to suggest a fountain model for the SMC. The O VI observations are consistent with this interpretation. This model is closely related to the supershell scenario discussed above, with the key difference being whether the hot gas is located in the main body of the SMC or in the halo. Ikeuchi & Norman (1987) and Norman & Ikeuchi (1989) state that a burst of star formation in a dwarf galaxy will form a superbubble that will easily break out into the halo because the gravitational potential is small, so it is reasonable to expect a fountain to exist in a star-forming dwarf galaxy like the SMC.

Using the model of Edgar & Chevalier (1986) for gas radiatively cooling from $T \gtrsim 10^6$ K, it is possible to roughly estimate the mass flow rate implied by the O VI column density. The expression for the mass flow rate \dot{M}/Ω is

$$\frac{\dot{M}}{\Omega} \approx (\mu m_{\text{H}}) n_{\text{H}0} \left(\frac{\dot{N}}{n_{\text{H}0}} \right), \quad (1)$$

where μm_{H} is the mean mass per atom, $n_{\text{H}0}$ is the initial density of ionized hydrogen in the cooling gas, Ω is the surface area of the fountain region, and \dot{N} is the flux of cooling gas in units of hydrogen ions $\text{cm}^2 \text{s}^{-1}$. Edgar & Chevalier find that under isobaric conditions $\dot{N}/n_{\text{H}0} \sim 2.5 \times 10^6 [N_{\perp}(\text{O VI})/10^{14} \text{cm}^{-2}]$. Using the mean O VI column density in Table 4 leads to a mass flow per unit surface area of

$$\frac{\dot{M}}{\Omega} \approx 2 \times 10^{-2} \left(\frac{n_{\text{H}0}}{10^{-2} \text{cm}^{-3}} \right) \text{M}_{\odot} \text{yr}^{-1} \text{kpc}^{-2}. \quad (2)$$

We leave $n_{\text{H}0}$ as an unknown, as there is no reliable way to estimate this for the SMC. Similarly, an estimate of the surface area of the SMC is very difficult to make in light of the irregular morphology and unknown orientation of the galaxy. Our estimate for the mass flow per unit area is probably similar to the number that would be derived for the Milky Way, since the O VI column densities are similar (to within a factor of 2). A more detailed discussion of this type of calculation can be found in Howk et al. (2002).

If the O VI is in front of both low ionization components, it is falling toward the SMC. This might occur if the hot gas were stripped out of the SMC by the gravitational interaction with the Milky Way, and is now falling back on the SMC. Sembach et al. (2000) found that the Magellanic Stream contains a high column of O VI ($\log N(\text{O VI}) \approx 14.62$), comparable to the columns seen in the SMC. This would naturally explain the

observed velocity shifts. It does not, however, explain the observed spatial correlation between high O VI column density and star-forming regions.

A clearer understanding of the origin of hot gas in the SMC might be gained by comparing O VI to other high ions, such as C IV, Si IV, and N V. Unfortunately, very little work has been done on these ions in the SMC with *HST*, so most of the available information is from *IUE* spectra. The low signal-to-noise of the *IUE* spectra make the determination of accurate column densities difficult. Table 5 lists the ratios of the column densities of high ions for the four *FUSE* stars with reliable *IUE* measurements. Of the four sight lines, the gas toward AV235 appears to be in the highest ionization state. However, AV229 and AV232 are in a star-forming region where appreciable C IV and Si IV may be produced locally. Sk 188 is a Wolf-Rayet star, which might also lead to C IV and Si IV production. Thus, the limited *IUE* data for C IV and Si IV do not allow a discrimination between the possible origins of the highly ionized gas in the SMC.

A STIS spectrum of one SMC sight line, AV229 (HD 5980), has been analyzed by Koenigsberger et al. (2001) and Hoopes et al. (2001). This sight line passes through an SNR in the SMC, but the SNR absorption is well separated from the SMC absorption. Hoopes et al. (2001) showed that the C IV/O VI and C IV/N V ratios in the general ISM along this sight line are in the range of the Milky Way halo ratios, implying that the processes producing the hot gas in the two galaxies are similar. The ratios in the SNR absorption were found to agree well with those predicted for evolved supernova remnants, and were different from the general ISM ratios in the SMC, suggesting that not all of the hot gas is in the form of cooling SNRs. AV229 is a Luminous Blue Variable/Wolf-Rayet binary star and is in a large H II region, so there may be local factors affecting the C IV and O VI abundance. The *FUSE* data toward Sk 108 indicate that the C IV/O VI ratio is several times higher than the Milky Way halo, suggesting that the ratio varies widely in the SMC (Mallouris et al. 2001). A systematic survey of high ion absorption in the SMC with STIS would be useful for studying the origin of highly ionized gas.

6. Conclusions

In this paper we have described the properties of O VI absorption along 18 sight lines in the Small Magellanic Cloud, using far ultraviolet spectra obtained with *FUSE*. The main results are:

1. Absorption from O VI is seen along every sight line in the SMC. The sight lines range in environment from star-forming regions (*e.g.*, NGC 346) to the field (*e.g.*, AV423), and includes the periphery of the SMC (Sk 188). The occurrence of O VI absorption in every direction indicates the presence of a widespread component of coronal temperature gas in the SMC.
2. The average column density is $\log N(\text{O VI}) \sim 14.53$. This is about 1.7 times higher than the Milky Way average of the column density perpendicular to the plane of $\log N(\text{O VI}) \sim 14.29$ (Savage et al. 2000). However, if NGC 346 is excluded, the average for the rest of the SMC falls to ~ 14.45 , only 1.4 times higher than the Galactic average.
3. The column density is correlated with position in the SMC. The highest values are seen toward the star-forming region NGC 346, and to a lesser extent toward the star-forming regions in the southwestern end of the Bar. Lower values are seen in the central region and in the Wing, where there is little star formation activity. This suggests that local processes strongly affect the hot gas distribution in the SMC, particularly in NGC 346.

4. The O VI line widths are broader than expected for pure thermal broadening, indicating that either non-thermal motions are prevalent, or that there are multiple components of hot gas at different velocities. The SMC O VI line widths are broader than the Milky Way O VI lines.
5. The kinematics suggest that the O VI is not associated with the gas producing the bulk of the low ionization absorption at $\sim +130 \text{ km s}^{-1}$. The O VI velocity is closer that of the $\sim +180 \text{ km s}^{-1}$ low ionization component, but evidence for a physical association is not conclusive. We discuss several mechanisms that may explain the observations, with superbubbles and/or a galactic fountain being the most probable.
6. If a galactic fountain is responsible for producing the hot gas, the rate of mass flow per unit surface area of the flow region is $\dot{M}/\Omega \sim 2 \times 10^{-2} \text{ M}_{\odot} \text{ yr}^{-1} \text{ kpc}^{-2}$, assuming an initial gas density of 10^{-2} cm^{-2} , which is very uncertain. Since the O VI column density in the SMC is within a factor of 2 of that of the Milky Way, the mass flow rates are probably similar if other conditions are the same.

We thank the anonymous referee for helpful comments. This work is based on data obtained for the Guaranteed Time Team by the NASA-CNES-CSA FUSE mission operated by the Johns Hopkins University. Financial support has been provided by NASA contract NAS5-32985. The SMC H α image was taken from the Southern H-Alpha Sky Survey Atlas (SHASSA), which is supported by the National Science Foundation. KRS and JCH acknowledge partial financial support from Long Term Space Astrophysics grant NAG5-3485.

REFERENCES

- Azzopardi, M., & Vigneau, J. 1982, A&AS, 50, 291
- Barlow, M. J., & Hummer, D. G. 1982, IAU Symp. 99: Wolf-Rayet Stars: Observations, Physics, Evolution, 99, 387
- Borkowski, K. J., Balbus, S. A., & Fristrom, C. C. 1990, ApJ, 355, 501
- Danforth, C. W., Howk, J. C. Fullerton, A. W., Blair, W. P., and Sembach, K. R. 2002, ApJS, in press [astro-ph/0110515]
- de Boer, K. S., & Savage, B. D. 1980, ApJ, 238, 86
- Edgar, R. J., & Chevalier, R. A. 1986, ApJ, 310, L27
- Fitzpatrick, E. L. 1984, ApJ, 282, 436
- Fitzpatrick, E. L. 1985, ApJS, 59, 77
- Fitzpatrick, E. L., & Savage, B. D. 1983, ApJ, 267, 93
- Fitzpatrick, E. L., & Savage, B. D. 1985, ApJ, 292, 122
- Garmany, C. D., Conti, P. S., & Massey, P. 1987, AJ, 93, 1070
- Gaustad, J. E., McCullough, P. R., Rosing, W., & Van Buren, D. 2001, PASP, 113, 1326
- Groenewegen, M. A. T. 2000, A&A, 363, 901

- Hoopes, C. G., Sembach, K. R., Howk, J. C., & Blair, W. P. 2001, *ApJ*, 558, L35
- Howk, J. C., Sembach, K. R., Savage, B. D., Massa, D., Friedman, S. D. & Fullerton, A. W. 2002, in preparation.
- Hurwitz, M., & Bowyer, S. 1996, *ApJ*, 465, 296
- Hurwitz, M., et al. 1998, *ApJ*, 500, L61
- Ikeuchi, S., & Norman, C. A. 1987, *ApJ*, 312, 485
- Jenkins, E. B. 1978a, *ApJ*, 219, 845
- Jenkins, E. B. 1978b, *ApJ*, 220, 107
- Jenkins, E. B., & Meloy, D. A. 1974, *ApJ*, 193, L121
- Kennicutt, R. C., & Hodge, P. W. 1986, *ApJ*, 306, 130
- Kennicutt, R. C., Bresolin, F., Bomans, D. J., Bothun, G. D., & Thompson, I. B. 1995, *AJ*, 109, 594
- Koenigsberger, G., et al. 2001, *AJ*, 121, 267
- Kunkel, W. E., Demers, S., & Irwin, M. J. 2000, *AJ*, 119, 2789
- Lehner, N., Fullerton, A. W., Sembach, K. R., Massa, D. L., & Jenkins, E. B. 2001, *ApJ*, 556, L103
- Mallouris, C., et al. 2001, *ApJ*, 558, 133
- Massey, P., Parker, J. W., & Garmany, C. D. 1989, *AJ*, 98, 1305
- Mathewson, D. S., Ford, V. L., & Visvanathan, N. 1986, *ApJ*, 301, 664
- Mathewson, D. S., Ford, V. L., & Visvanathan, N. 1988, *ApJ*, 333, 617
- McGee, R. X., & Newton, L. M. 1981, *Proceedings of the Astronomical Society of Australia*, 4, 189
- McKee, C. F., & Ostriker, J. P. 1977, *ApJ*, 218, 148
- Moos, H. W., et al. 2000, *ApJ*, 538, L1
- Norman, C. A., & Ikeuchi, S. 1989, *ApJ*, 345, 372
- Sanduleak, N. 1968, *AJ*, 73, 246
- Sanduleak, N. 1969, *AJ*, 74, 877
- Savage, B. D., et al. 2000, *ApJ*, 538, L27
- Sembach, K. R., et al. 2000, *ApJ*, 538, L31
- Sembach, K. R., & Savage, B. D. 1992, *ApJS*, 83, 147
- Sembach, K. R., Savage, B. D., & Hurwitz, M. 1999, *ApJ*, 524, 98
- Sembach, K. R., Howk, J. C., Savage, B. D., Shull, J. M., & Oegerle, W. R. 2001, *ApJ*, 561, 573

- Shull, J. M., & McKee, C. F. 1979, *ApJ*, 227, 131
- Slavin, J. D., Shull, J. M., & Begelman, M. C. 1993, *ApJ*, 407, 83
- Spitzer, L. J. 1956, *ApJ*, 124, 20
- Spitzer, L. 1990, *ARA&A*, 28, 71
- Staveley-Smith, L., Sault, R. J., Hatzidimitriou, D., Kesteven, M. J., & McConnell, D. 1997, *MNRAS*, 289, 225
- Sterling, N. C., Savage, B. D., Richter, P., Fabian, D., & Sembach, K. R. 2001, *ApJ*, in press [astro-ph/0111226]
- Sutherland, R. S., & Dopita, M. A. 1993, *ApJS*, 88, 253
- Walborn, N. R. 1977, *ApJ*, 215, 53
- Walborn, N. R., & Blades, J. C. 1986, *ApJ*, 304, L17
- Walborn, N. R., et al. 2001a, *AJ*, submitted
- Wang, Q. 1991, *ApJ*, 377, L85
- Walborn, N. R., Lennon, D. J., Haser, S. M., Kudritzki, R., & Voels, S. A. 1995, *PASP*, 107, 104
- Walborn, N. R., Lennon, D. J., Heap, S. R., Lindler, D. J., Smith, L. J., Evans, C. J., & Parker, J. W. 2000, *PASP*, 112, 1243
- Walborn, N. R., Fullerton, A. W., Crowther, P. A., et al. 2001b, in prep.
- Wang, Q. D. 1999, *ApJ*, 510, L139
- Wang, Q., & Wu, X. 1992, *ApJS*, 78, 391
- Welch, D. L., McLaren, R. A., Madore, B. F., & McAlary, C. W. 1987, *ApJ*, 321, 162
- Widmann, H., et al. 1998, *A&A*, 338, L1
- Williams, R. M., & Chu, Y. 1995, *ApJ*, 439, 132

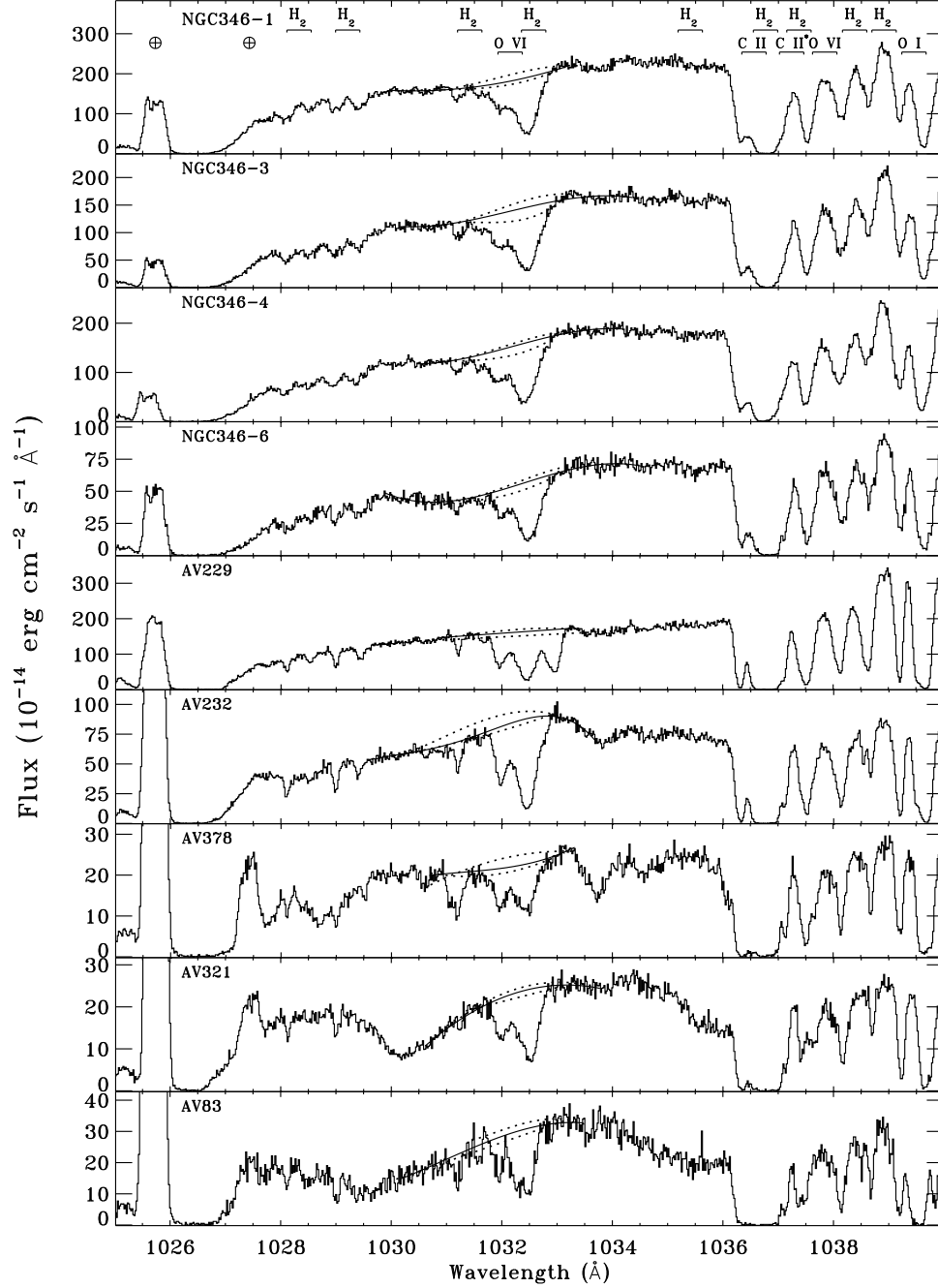
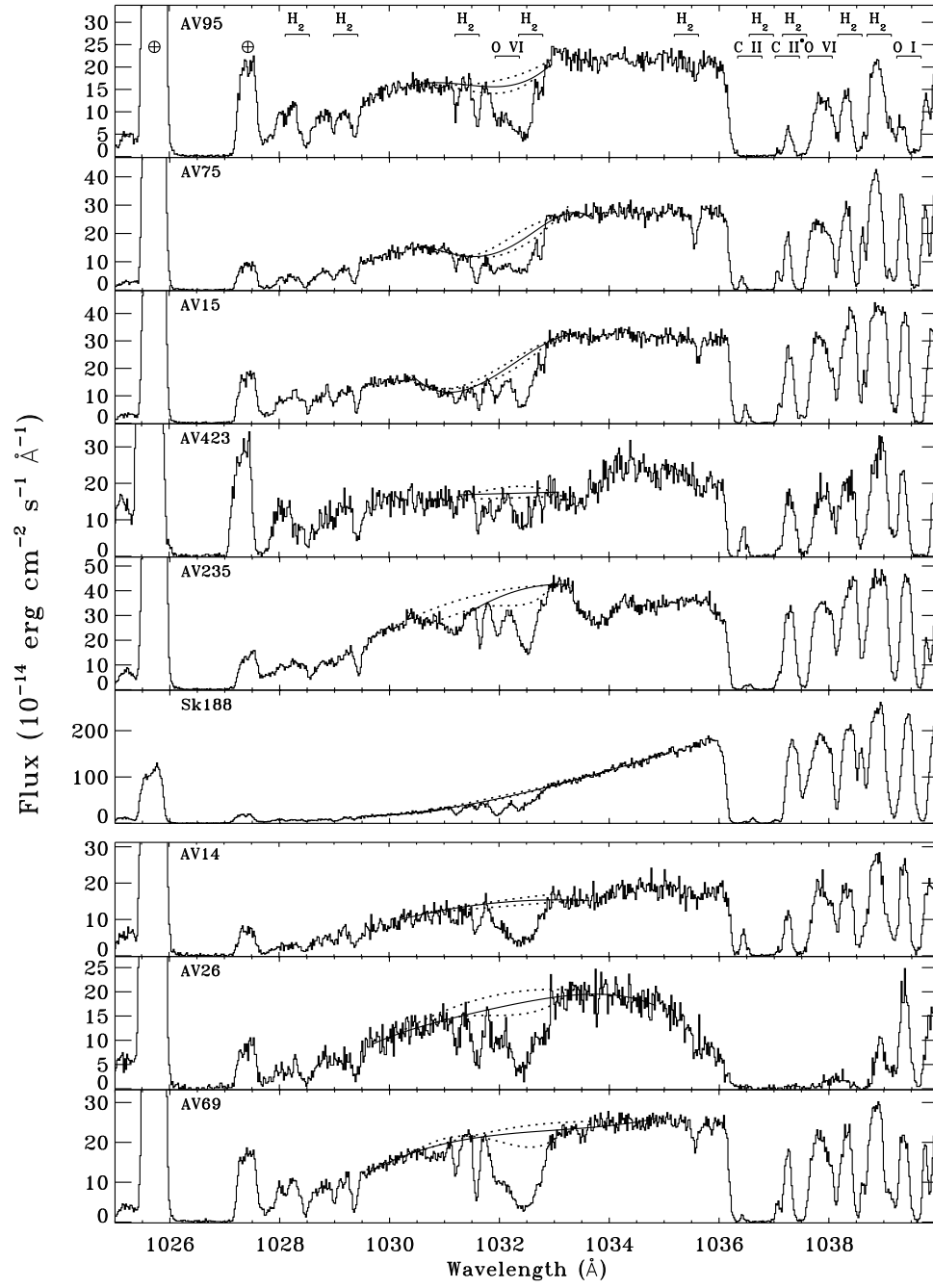


Fig. 1.— The observed *FUSE* spectra of the sample stars near the O VI lines. Atomic and H_2 lines in the Galactic and SMC rest frames are identified in the top panel. The adopted continuum over the O VI 1031.93 \AA line is shown as a solid line, and the maximum and minimum continua used to determine the continuum placement uncertainty are shown as dashed lines. The spectra of AV14, AV26, and AV69 are separated from the rest as they may suffer from contamination by stellar absorption.



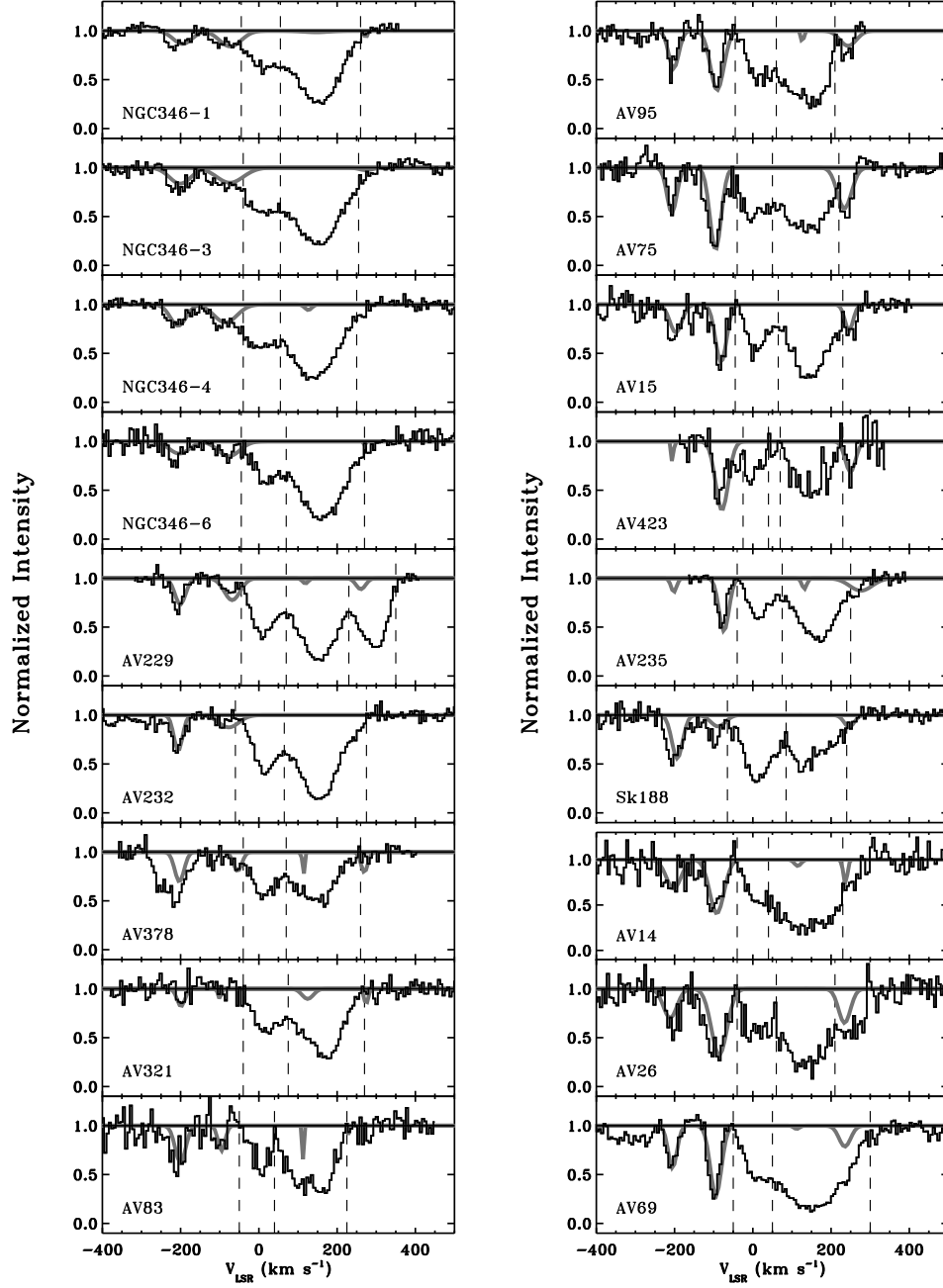


Fig. 2.— The continuum-normalized O VI profiles. The thick grey lines are the predicted strengths of the H₂ 6-0 P(3) 1031.19 Å and 6-0 R(4) 1032.35 Å lines. The predictions are based on nearby lines from the same rotational level. The vertical dashed lines show the velocity integration limits used to measure equivalent widths and column densities. The profiles for AV14, AV26, and AV69 are separated from the rest as they may suffer from contamination by stellar absorption.

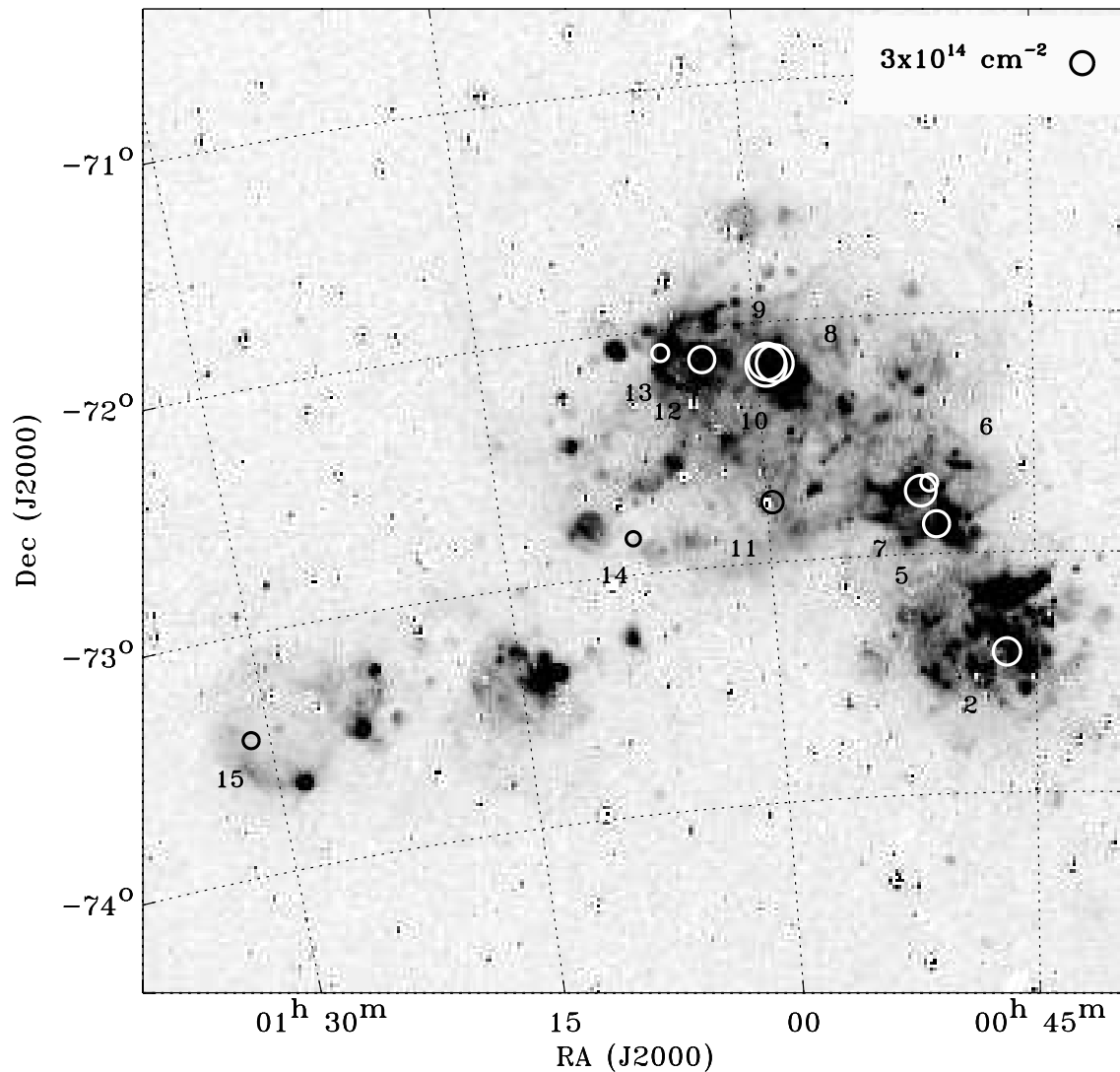


Fig. 3.— $H\alpha$ image of the SMC (Gaustad et al. 2001) with the positions of the sight lines marked. The radius of the circle used to mark each star is linearly proportional to the column density of O VI in the SMC. A circle corresponding to $N(\text{O VI})=3 \times 10^{14} \text{ cm}^{-2}$ is shown in the upper right corner. The numbers given beside each circle correspond to the identifications listed in Table 1. AV14, AV26, and AV69 are not shown as the measured column densities toward these stars are unreliable. They are located in the southwestern end of the Bar, near star 5 (AV75). The four stars in NGC 346 are labeled as one (star 8) as they are very close together.

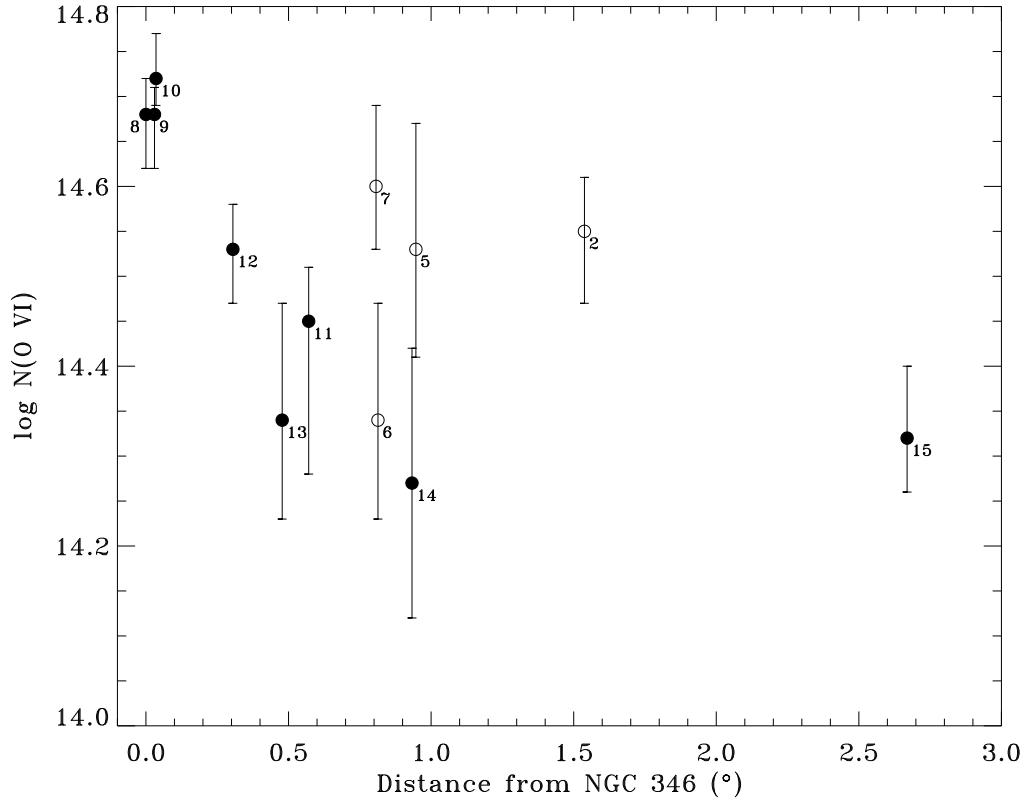


Fig. 4.— The measured O VI column densities plotted as a function of distance from NGC 346. The average value for the stars in NGC 346 is shown (point 8). The column density toward AV229 (point 9) does not include the contribution from the SNR observed along the sight line. The open circles represent the stars in the southwestern end of the Bar, where star formation is occurring. The error bars shown include both random and systematic (continuum fit) uncertainty. Unreliable values for several stars (AV69, AV14, and AV26) are not shown.

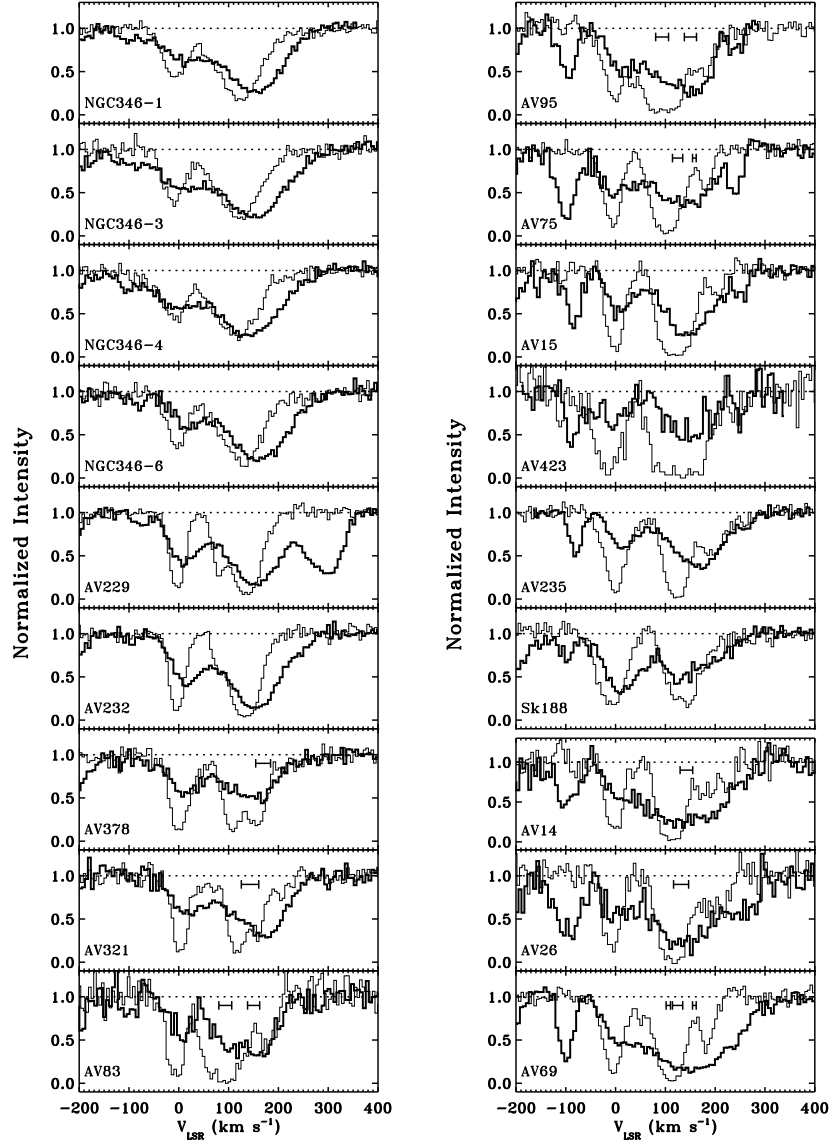


Fig. 5.— The continuum-normalized O VI profiles compared to Fe II 1144.94 Å absorption in velocity space. The O VI absorption is shown by the thick line, while the Fe II profile is shown by the thin line. The velocity scale is set so that the Milky Way Fe II absorption falls at 0 km s^{-1} . The SMC absorption lies between $\sim +100$ and $+200 \text{ km s}^{-1}$, and often consists of two components in the Fe II line. The absorption at -100 and $+260 \text{ km s}^{-1}$ seen in some of the O VI spectra is caused by the 6-0 P(3) and 6-0 R(4) levels of H_2 in the SMC, respectively. The O VI absorption at $+300 \text{ km s}^{-1}$ toward AV229 is caused by a supernova remnant in the line of sight (Hoopes et al. 2001). The horizontal error bars denote the velocities of identified shells along the sight line, from the catalog of Staveley-Smith et al. (1997). The left and right ends of each error bar mark the velocities of the approaching and receding sides of each shell, respectively. The profiles for AV14, AV26, and AV69 are separated from the rest as they may suffer from contamination by stellar absorption.

Table 1. Information on Observed Stars

ID ^a	Star	Alternate Names	l ($^{\circ}$)	b ($^{\circ}$)	α_{2000} (h m s)	δ_{2000} ($^{\circ}$ ' ")	Type ^b	HII Region ^c
1	AV14	Sk 9	303.43	−44.02	00:46:32.66	−73:06:05.6	O3-4V	N12
2	AV15	Sk 10	303.40	−43.71	00:46:42.19	−73:24:54.7	O6.5II(f)	...
3	AV26	Sk 18	303.30	−43.99	00:47:50.07	−73:08:20.7	O7III	N19
4	AV69	Sk 34	303.05	−44.24	00:50:17.40	−72:53:29.9	OC7.5III((f))	N36
5	AV75	Sk 38	303.02	−44.25	00:50:32.50	−72:52:36.2	O5III(f+)	N36
6	AV83	...	302.99	−44.42	00:50:52.01	−72:42:14.5	O7Iaf+	...
7	AV95	...	302.94	−44.39	00:51:21.54	−72:44:12.9	O7III((f))	...
8	NGC 346-6	MPG#324	302.12	−44.94	00:58:57.74	−72:10:33.6	O4V((f))	N66
8	NGC 346-4	MPG#342	302.11	−44.94	00:59:00.39	−72:10:37.9	O5-6V	N66
8	NGC 346-3	MPG#355	302.11	−44.94	00:59:01.09	−72:10:28.2	O2III(f*)	N66
8	NGC 346-1	MPG#435	302.11	−44.94	00:59:04.81	−72:10:24.8	O4III(n)(f)	N66
9	AV229	Sk 78, HD5980	302.07	−44.95	00:59:26.70	−72:09:55.0	OB?+WN3	N66B
10	AV232	Sk 80	302.06	−44.94	00:59:30.00	−72:11:00.0	O7Iaf+	N66
11	AV235	Sk 82	302.07	−44.37	00:59:42.00	−72:45:00.0	B0Iw	...
12	AV321	...	301.68	−44.96	01:02:57.04	−72:08:09.3	B0IIIw	...
13	AV378	...	301.44	−45.00	01:05:09.44	−72:05:35.0	O8V	...
14	AV423	Sk 132	301.26	−44.23	01:07:40.43	−72:50:59.6	O9.5II(n)	...
15	Sk 188	AB8	299.06	−43.41	01:31:06.00	−73:26:00.0	WO4+O7III	...

^aStar identification number used in Figures 3 and 4.

^bSpectral types were taken from Walborn 1977; Barlow & Hummer 1982; Walborn & Blades 1986; Garmany et al. 1987; Walborn et al. 1995, 2000, 2001a, 2001b.

^cThe HII region designations are from Henize 1956.

Table 2. FUSE Observations

Star	Date	FUSE dataset ID ^a	Exposure Time (ks)
AV14	2000 Jul 1	P11753	6.8
AV15	2000 May 30	P11501	14.6
AV26	2000 Jul 2	P11760	4.0
AV69	2000 May 31	P11503	17.6
AV75	2000 May 31	P11504	14.4
AV83	2000 Jul 2	P11762	4.0
AV95	2000 May 31	P11505	14.3
NGC 346-6	2000 Oct 1	P11756	5.9
NGC 346-4	2000 Sep 30	P11757	5.0
NGC 346-3	2000 Oct 1	P11752	5.1
NGC 346-1	2000 Oct 11	P11755	5.6
AV229	2000 Jul 2	P10301	5.5
AV232	2000 Jul 2	P10302	11.7
AV235	2000 Jul 2	P10303	16.2
AV321	2000 Jun 1	P11506	16.9
AV378	2000 Jun 1	P11507	14.7
AV423	2000 Oct 10	P11767	3.5
Sk 188	2000 Oct 11	P10306	6.9

^aThe data are archived in the Multimission Archive at the Space Telescope Science Institute.

Table 3. Measured Properties of the Galactic O VI Absorption

ID ^a	Star	Velocity range (km s ⁻¹)	W_λ (O VI) ^b (mÅ)	$\log N(\text{O VI})^b$ (cm ⁻²)	$\langle v \rangle^c$ (km s ⁻¹)	Δv^c (km s ⁻¹)
1	AV14 ^d	-40, +40	102 ± 12 ⁺⁴ ₋₁₉	14.02 ± 0.08 ^{+0.03} _{-0.08}	11 ± 3	47 ± 5
2	AV15	-45, +65	110 ± 12 ⁺²⁶ ₋₂₀	14.04 ± 0.06 ^{+0.11} _{-0.10}	16 ± 4	54 ± 7
3	AV26 ^d	-40, +60	127 ± 15 ⁺³⁰ ₋₂₄	14.12 ± 0.07 ^{+0.12} _{-0.10}	13 ± 4	59 ± 7
4	AV69 ^d	-50, +50	144 ± 7 ⁺¹⁰ ₋₁₂	14.20 ± 0.04 ^{+0.04} _{-0.05}	13 ± 3	56 ± 7
5	AV75	-40, +50	134 ± 14 ⁺²⁷ ₋₁₇	14.15 ± 0.07 ^{+0.12} _{-0.07}	8 ± 2	56 ± 5
6	AV83	-50, +40	84 ± 11 ⁺¹⁶ ₋₁₈	13.93 ± 0.07 ^{+0.08} _{-0.14}	4 ± 4	42 ± 7
7	AV95	-45, +60	130 ± 20 ⁺¹⁸ ₋₂₅	14.14 ± 0.07 ^{+0.07} _{-0.11}	19 ± 5	56 ± 9
8	NGC 346-1	-45, +55	115 ± 10 ⁺¹⁷ ₋₁₀	14.05 ± 0.04 ^{+0.05} _{-0.05}	10 ± 3	64 ± 9
8	NGC 346-3	-40, +55	140 ± 6 ⁺¹² ₋₂₆	14.16 ± 0.04 ^{+0.05} _{-0.11}	9 ± 2	61 ± 7
8	NGC 346-4	-40, +55	137 ± 5 ⁺⁶ ₋₂₄	14.15 ± 0.04 ^{+0.02} _{-0.11}	9 ± 2	64 ± 9
8	NGC 346-6	-40, +65	112 ± 8 ⁺⁶ ₋₂₇	14.04 ± 0.05 ^{+0.03} _{-0.13}	22 ± 3	61 ± 7
9	AV229	-45, +70	164 ± 5 ⁺¹⁰ ₋₃₉	14.25 ± 0.03 ^{+0.03} _{-0.06}	17 ± 2	64 ± 5
10	AV232	-60, +65	155 ± 6 ⁺³¹ ₋₁₂	14.23 ± 0.03 ^{+0.09} _{-0.05}	19 ± 3	61 ± 5
11	AV235	-40, +75	101 ± 12 ⁺²² ₋₃₀	13.98 ± 0.06 ^{+0.12} _{-0.16}	22 ± 4	64 ± 9
12	AV321	-40, +75	130 ± 8 ⁺¹⁰ ₋₁₁	14.11 ± 0.05 ^{+0.04} _{-0.04}	24 ± 3	66 ± 5
13	AV378	-40, +70	124 ± 12 ⁺¹⁴ ₋₁₆	14.09 ± 0.06 ^{+0.06} _{-0.08}	17 ± 3	64 ± 7
14	AV423	-25, +40	61 ± 11 ⁺¹³ ₋₁₄	13.77 ± 0.10 ^{+0.10} _{-0.12}	4 ± 3	40 ± 5
15	Sk 188	-65, +85	215 ± 9 ⁺²³ ₋₁₂	14.39 ± 0.03 ^{+0.05} _{-0.04}	17 ± 2	78 ± 5
Mean ^e	126 ± 37	14.12 ^{+0.13} _{-0.18}	15 ± 6	58 ± 10
Mean ^f	128 ± 39	14.12 ^{+0.14} _{-0.20}	15 ± 7	58 ± 10

^aStar identification number used in Figures 3 and 4.

^bThe first uncertainty includes statistical and velocity range errors, and the second is due to continuum placement errors.

^cThe mean velocity is the first moment of the line, so the statistics are weighted by the data values. The width is the second moment multiplied by 2.35, or roughly the FWHM.

^dStellar absorption may affect the measurement of the interstellar absorption toward AV69, AV14, and AV26.

^eThe NGC 346 values were averaged together and treated as one measurement in the global mean. AV69 is not included in this mean.

^fThe NGC 346 values were averaged together and treated as one measurement in the global mean. AV69, AV14, and AV26 are not included in this mean.

Table 4. Measured Properties of the SMC O VI Absorption

ID ^a	Star	Velocity range (km s ⁻¹)	W_λ (O VI) ^b (mÅ)	$\log N(\text{O VI})^b$ (cm ⁻²)	$\langle v \rangle^c$ (km s ⁻¹)	Δv^c (km s ⁻¹)
Northern Bar near NGC 346						
8	NGC 346-1	+55, +260	349 ± 10 $^{+26}_{-15}$	14.63 ± 0.02 $^{+0.04}_{-0.02}$	148 ± 3	106 ± 5
8	NGC 346-3	+55, +255	395 ± 8 $^{+24}_{-13}$	14.71 ± 0.02 $^{+0.04}_{-0.07}$	148 ± 2	108 ± 5
8	NGC 346-4	+55, +250	361 ± 8 $^{+31}_{-14}$	14.67 ± 0.02 $^{+0.01}_{-0.07}$	142 ± 2	104 ± 5
8	NGC 346-6	+65, +270	377 ± 10 $^{+15}_{-10}$	14.69 ± 0.02 $^{+0.02}_{-0.05}$	160 ± 2	104 ± 5
9	AV229	+70, +350	555 ± 12 $^{+12}_{-34}$	14.86 ± 0.03 $^{+0.02}_{-0.05}$
9	AV229 ^d	+70, +230	345 ± 7 $^{+9}_{-17}$	14.68 ± 0.02 $^{+0.01}_{-0.04}$	151 ± 2	97 ± 7
10	AV232	+65, +275	384 ± 8 $^{+18}_{-10}$	14.72 ± 0.02 $^{+0.03}_{-0.01}$	153 ± 2	97 ± 5
Northern Bar outside NGC 346						
13	AV378	+70, +260	211 ± 17 $^{+31}_{-17}$	14.34 ± 0.05 $^{+0.08}_{-0.06}$	149 ± 4	101 ± 9
12	AV321	+75, +270	290 ± 9 $^{+13}_{-18}$	14.53 ± 0.03 $^{+0.02}_{-0.03}$	160 ± 2	94 ± 5
Southwestern Bar						
6	AV83	+40, +225	296 ± 15 $^{+20}_{-10}$	14.34 ± 0.05 $^{+0.08}_{-0.06}$	133 ± 3	97 ± 5
7	AV95	+60, +210	313 ± 18 $^{+29}_{-15}$	14.60 ± 0.04 $^{+0.06}_{-0.03}$	135 ± 3	89 ± 7
4	AV69 ^e	+50, +300	544 ± 11 $^{+22}_{-53}$	14.90 ± 0.02 $^{+0.03}_{-0.07}$	155 ± 2	131 ± 5
5	AV75	+50, +220	298 ± 16 $^{+44}_{-22}$	14.53 ± 0.04 $^{+0.10}_{-0.08}$	133 ± 3	97 ± 5
3	AV26 ^e	+60, +210	344 ± 15 $^{+27}_{-22}$	14.68 ± 0.05 $^{+0.05}_{-0.05}$	135 ± 3	87 ± 5
1	AV14 ^e	+40, +230	435 ± 15 $^{+11}_{-19}$	14.77 ± 0.04 $^{+0.02}_{-0.03}$	134 ± 3	115 ± 5
2	AV15	+65, +230	291 ± 11 $^{+14}_{-26}$	14.55 ± 0.03 $^{+0.03}_{-0.05}$	146 ± 2	85 ± 5
Center						
14	AV423	+70, +230	174 ± 19 $^{+35}_{-30}$	14.27 ± 0.06 $^{+0.09}_{-0.09}$	146 ± 5	82 ± 7
11	AV235	+75, +250	256 ± 14 $^{+30}_{-56}$	14.45 ± 0.04 $^{+0.02}_{-0.13}$	163 ± 4	94 ± 9
Wing						
15	Sk 188	+85, +240	202 ± 7 $^{+17}_{-9}$	14.32 ± 0.03 $^{+0.05}_{-0.03}$	153 ± 2	92 ± 5
Global Properties						
Mean ^f	300 ± 73	14.56 $^{+0.14}_{-0.20}$	145 ± 10	94 ± 8
Mean ^g	286 ± 66	14.53 $^{+0.13}_{-0.19}$	147 ± 10	93 ± 6

^aStar identification number used in Figures 3 and 4.

^bThe first uncertainty includes statistical and velocity range errors, and the second is due to continuum placement errors.

^cThe mean velocity is the first moment of the line, so the statistics are weighted by the data values. The width is the second moment multiplied by 2.35, or roughly the FWHM.

^dThis measurement excludes the SNR.

^eStellar absorption may affect the measurement of the interstellar absorption toward AV69, AV14, and AV26.

^fThe NGC 346 values were averaged together and treated as one measurement in the global mean. AV69 is not included in this mean. The SNR is excluded.

^gThe NGC 346 values were averaged together and treated as one measurement in the global mean. AV69, AV14, and AV26 are not included in this mean. The SNR is included.

Table 5. High Ion Column Density Ratios^a

Star	N(Si IV) λ 1402/N(O VI)	N(C IV) λ 1550/N(O VI)
AV229	0.27 – 0.30	0.62 – 0.70
AV232	0.19 – 0.25	0.25 – 0.37
AV235	0.08 – 0.20	≥ 0.15
Sk 188	0.13 – 0.23	0.34 – 0.57

^aColumn densities were calculated from the equivalent widths in Fitzpatrick & Savage 1985, except O VI column densities from this paper. The column densities for AV229 were remeasured from the data used by Koenigsberger et al. 2001.